JMEPEG (2012) 21:540–547
DOI: 10.1007/s11665-011-9948-6

1059-9495/$19.00

Role of Welding Parameters Using the Flux Cored Arc Welding Process of Low Alloy Steels on Bead Geometry and Mechanical Properties

A. Aloraier, A. Almazrouee, T. Shehata, and John W.H. Price

(Submitted June 10, 2010; in revised form December 18, 2010)

Welding parameters have direct effects on the bead geometry, microstructure, and mechanical properties of low alloy steels. A series of experiments have been carried out to examine some of these parameters using the flux cored arc welding process (FCAW). In this article, an experimental study was conducted to investigate the influence of welding parameters in FCAW process particularly welding voltage and travel speed on weld bead dimensions. The study also includes the effects of bead overlap and deposition sequence on the parent material and the heat-affected zone (HAZ) properties. It was found that an increase in the welding voltage leads to an increase in the weld bead width, and the increase in the welding traverse speed leads to a decrease in the weld bead width. When studying the bead overlap percentages, it was found that the 50% bead overlap can be considered to be practically a better option than the higher percentages of bead overlap (i.e., 70-90%). The experimental investigation of studying the deposition sequence showed that there were no significant differences in the microstructure, hardness, and the size of the refined HAZ between the two proposed deposition sequences. However, a significant improvement in the microstructure and the size of the refined HAZ, and a reduction in the hardness were achieved after depositing the second welding bead, irrespective of the depositing sequence.

Keywords bead geometry, deposition sequence, heat-affected zone, overlap percentage, traverse speed

1. Introduction

Flux Cored Arc Welding (FCAW) is a high deposition rate process increasingly used in fabrication and repair (Ref 1-3). FCAW can provide better control over current and heat input (Ref 4, 5). Better control leads to better composition, dilution, and grain size, enhancing the mechanical properties of the used components. The welding pool is protected by the flux inside the tube and also often by shielding gases. The shielding gas can be either inert, like argon or active like CO_2, or a mixture of both. FCAW is a semi-automatic or fully automatic process and thus should also have cost advantages over the other commonly used processes.

The welding process and parameters plays a decisive role in controlling the bead geometry. Weld bead geometry is the first indication of the weld bead quality. It results from the solidification of liquid metal so that interfacial tensions determine the ultimate bead geometry (Ref 6, 7). The bead cross-sectional area affects the total shrinkage and, consequently, the residual stress and distortion (Ref 8). Controlling bead geometry is important for minimizing cracking susceptibility of weldments (Ref 9). Weld bead geometry plays an important and critical role in determining the mechanical properties of the welded structure (Ref 10).

Weld bead geometry includes the weld bead width (W), the weld bead height (H), or the weld bead reinforcement (R), and the depth of penetration (P). These elements, W, R, and P are sensitive to the welding input parameters, namely, welding voltage and traverse speed. Bead geometry and the microstructure of both weld metal and the heat-affected zone (HAZ) are affected to a great degree by these welding parameters. The relationship between arc welding parameters and weld bead geometry is complex, since a number of factors are involved (Ref 10-13). Therefore, the aim of this study is to provide an insight into the role of different welding parameters on the weld bead geometry, microstructure, and hardness of FCAW. These welding parameters include the welding voltage, the traverse speed, the bead's overlap percentage, and the bead deposition sequence. The practical significance of this study is found in achieving soundness integrity of welded components using FCAW.

2. Experimental Procedures

A series of experiments were carried out to investigate the welding parameters and their effects on bead geometry, microstructure, and hardness. A UNI-MIG 375 K welding machine was used with an ARGOSHIELD 52 (77% Ar + 23% CO_2) shielding gas. The specimens were mounted under an

A. Aloraier and **A. Almazrouee**, Mechanical Production Engineering Department, College of Technological Studies, PAAET, Kuwait City, Kuwait; **T. Shehata**, Mechanical Engineering Department, Taibah University, Taibah, Kingdom of Saudi Arabia; and **John W.H. Price**, Mechanical Engineering Department, Monash University, Clayton, VIC 3800, Australia. Contact e-mail: aloraier@gmail.com.

automatic speed-controlled welding torch. The aims of these experiments are as follows:

1. To study the effect of voltage and traverse speed on bead geometry;
2. To examine the effects of bead overlap on the microstructure and hardness; and
3. To investigate the effect of deposition sequence on the microstructure, size of the HAZ, and hardness.

2.1 Materials and Consumables

The bead-on-plate technique was used to perform the experiments as shown in Fig. 1(a). The parent material and the tubular welding wire used in this study were, respectively, low-carbon steel (AS 3678-250) and Super-COR 5 (conforming to AWS A5.20). The chemical composition and mechanical properties of both the parent material and consumable weld metal are shown in Tables 1 and 2, respectively.

2.2 Welding Parameters and Bead Geometry

Four welding traverse speeds (360, 420, 480, and 540 mm/min) with respective welding voltages (23, 25, 28, and 32 V) were employed using a tubular welding wire of 1.2 mm diameter. The plate was then left to cool down to ambient temperature. A coupon of 10 mm width was taken from the center of each specimen as shown in Fig. 1(a) and (b). The welding voltage and amperage were recorded during the welding process. Three samples were produced for each traverse speed and voltage to ensure repeatability. A wire-feeding rate of 3600 mm/min was used. Figure 1(b) shows the weld bead geometry elements: weld bead width (W), weld bead height (H), depth of penetration (P) and depth of HAZ (DHAZ). These elements were measured, and then were averaged for the three samples. Specimens were polished and etched using a 2% nital solution to reveal the microstructure and display the bead dimensions. Measurements of bead dimensions were carried out using a binocular microscope equipped with a calibrated reticule.

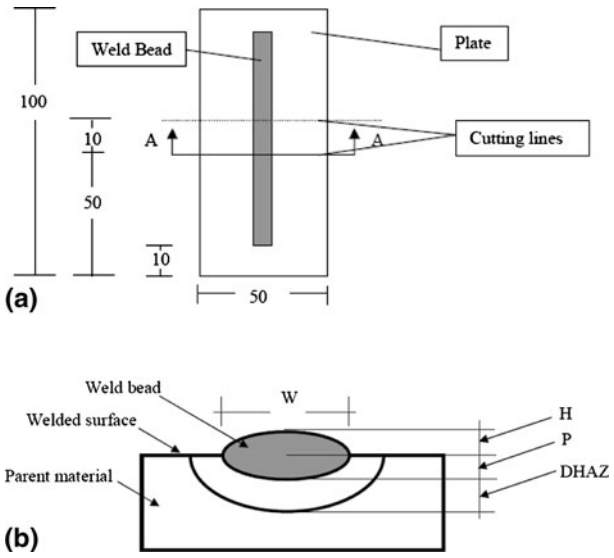

Fig. 1 Schematic illustration of (a) bead-on-plate and the section line of the studied specimen, and (b) weld bead geometry elements

2.3 Percentage of Bead Overlap

The aim of this experimental study in this and the next sections was to carry out welds following well-defined parameters and variables obtained from the results of the previous section. In this experimental study, two weld beads were deposited. The first weld bead was deposited in the center of the plate with a start-and-stop distances of 20 mm from each side of the parent material as shown in Fig. 2(a). The width of the weld beads varied from 12 mm at the start of welding to 14 mm at the end. The length of the weld bead was approximately 160 mm.

The second bead was deposited parallel to the first bead. This procedure differed from the previous study where the beads were inclined at an angle to each other (Ref 3). The second weld bead was deposited to one side of the first bead after the latter had cooled to ambient temperature. Different samples were produced by adjusting the tip of the electrode with respect to the width of the first bead, i.e., to achieve 50% of bead overlap the electrode tip was placed at the toe of the first bead. Five samples were produced (40-80%) of bead overlap. Figure 2(b) shows a schematic representation of the five samples produced. The samples which have overlap percentages of less than 40% and higher than 80% were excluded in this study based on the results of the previous study (Ref 4). Neither post-weld heat treatment nor preheating was performed in this study.

2.4 Deposition Sequence

Two deposition sequences were employed in this experimental study. In the first sequence, the first bead was deposited on the center of the parent material. The second bead deposition was located lateral to the first bead, such that half of the second bead overlapped the first bead by 50%. The third was deposited at a similar location with respect to the second bead. These three beads formed the first layer of the weld. The second layer, which consisted of one bead, was then deposited on the top of

Table 2 Mechanical properties of the parent material and consumable

Material	Yield stress, MPa	Tensile strength, MPa	Elongation, %
AS 3678-250	285	429	38
SUPER-COR5	445	550	29

Table 1 Chemical composition of the parent and weld metals using ARGOSHIELD 52 shield gas

Elements	C	Si	Mn	P	S	Cr	Ni	Mo	V
Parent material	0.12	0.13	0.63	0.02	0.01	0.01	0.02	<0.01	<0.01
Consumable	0.10	0.68	1.73	0.019	0.017	0.03	0.05	0.04	0.04

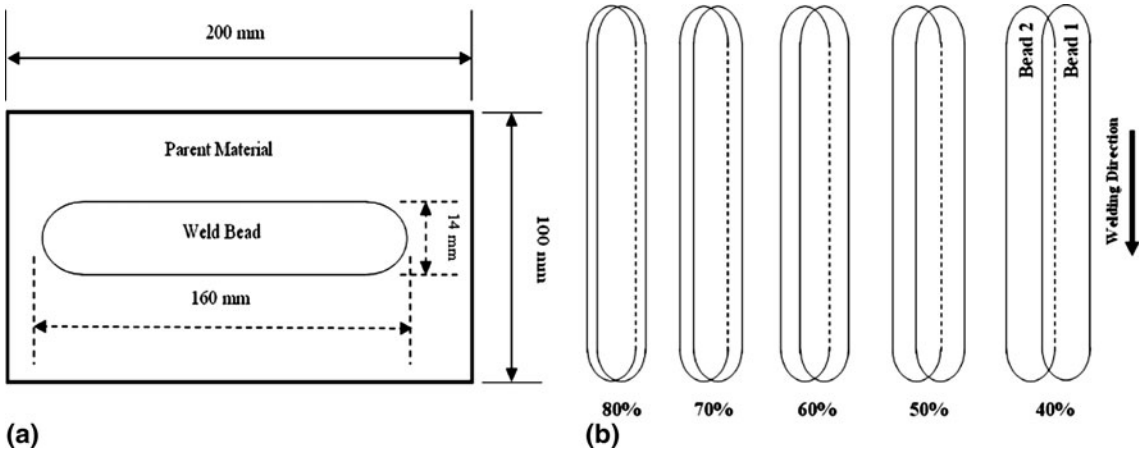

Fig. 2 Schematic illustration of (a) position of the first bead and (b) different overlap percentages

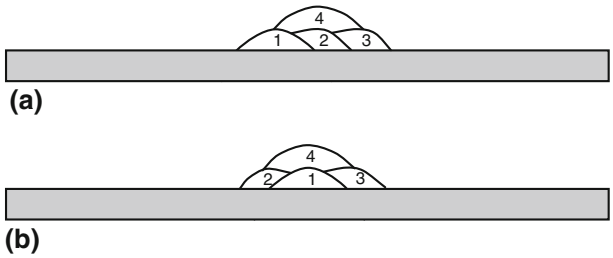

Fig. 3 Schematic illustration: (a) first sequence, and (b) second sequence

the first layer. In the second deposition sequence, the first two steps were identical to those in the first sequence. The third bead was deposited on the other side of the first bead and opposite to the location of the second bead. These three beads form the first layer and overlap the previous bead by 50%. The top layer was identical to the second layer of the first deposition sequence. A schematic illustration of both deposition sequences is shown in Fig. 3. Further explanations can be found in Ref 5.

The heat inputs were varied by changing the traverse speed of the weld gun, i.e., the first layers in both sequences were deposited with fast traverse speed, whereas the second layers deposited with slower ones. Table 3 shows the welding parameters used in the deposition sequence experiment.

2.5 Microstructure and Hardness

Transverse sections of the weldments were ground and polished to a 3 μm finish, and etched in Nital solution (2%) before microscopy. Microstructure variations across the weldments were characterized by reflected microscopy for both the percentage of bead overlap and the deposition sequence.

Hardness profiles across the HAZ with different percentages of bead overlap were obtained under 5 kg indentation load. These hardness measurements were employed to study the effects of overlap percentage and the deposition sequence.

To study the hardness of the HAZ which was produced by different bead overlap percentages, a traverse line from the center of the first bead to the toe was drawn on all the samples and adopted to measure the change in the hardness as shown in Fig. 4(a). This traverse line was drawn at a distance of 1 mm under the fusion line on all the samples with the same location and with the same dimensions.

For the deposition sequence, the hardness was also carried out on three vertical lines moving from the weld metal through the HAZ to the parent material as shown in Fig. 4(b) to study the effects of the subsequent bead on the weld metal, the HAZ, and the parent material of the previous bead. Hardness profile under different welding conditions were then generated and studied. It was ensured that the hardness traverse lines were drawn in all the samples with the same location and dimensions.

3. Results and Discussion

Welding voltage, traverse speed, and the type of shielding gas are critical parameters which affect the heat input, thereby affecting the melting rate of the base metal. As a result, any change in the previous welding parameters will change the amount and the shape of the melted pool which consequently alter the bead geometry. Furthermore, the percentage of bead overlap and the deposition sequence have significant effects on the mechanical properties and the microstructure of the HAZ, and they are considered to be very important factors in repair welding.

3.1 The Effects of Welding Parameters on Bead Geometry

The measured weld bead geometry elements are plotted against the welding voltages and the traverse speed as shown in Fig. 5 and 6, respectively. The effects of changing the welding voltage on the weld bead width are shown in Fig. 5(a). In general, the weld bead width increases with the increase in the welding voltage, at all welding traverse speeds. The results of this study is consistent with the previous studies (Ref 9, 14). The effect of the increase in the welding voltage on the weld bead height is shown in Fig. 5(b). The increase in the welding voltage leads to a decrease in the weld bead height. The highest decrease of the weld bead height with the increase in the welding voltage occurs at the highest welding traverse speed (540 mm/min). On the other hand, the highest values of the weld bead height were measured at the slowest welding

Table 3 Welding parameters used in the deposition sequence experimental study

Layer No.	Electrode diameter, mm	Current range, A	Voltage range, V	Traverse speed, mm/min	Wire feeding speed, mm/min	Electrode stick-out distance, mm	Gas flow rate, L/min
1	1.6	215-245	23-25	560	3600	20	20
2	1.6	215-245	23-25	290	3600	20	20

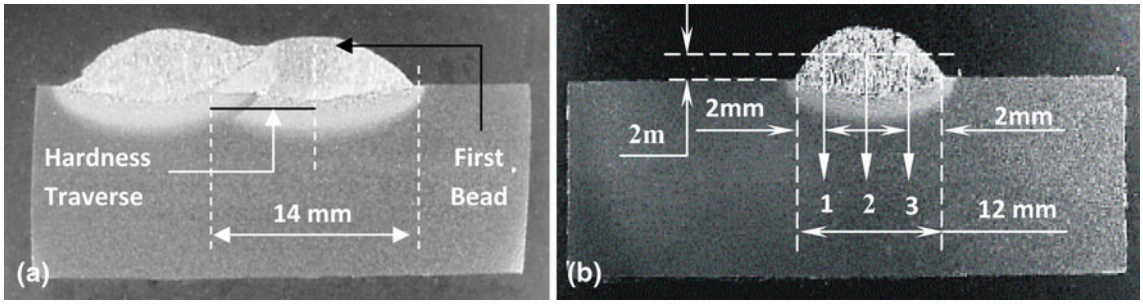

Fig. 4 Illustration of hardness measurements locations for (a) bead overlap, and (b) deposition sequence

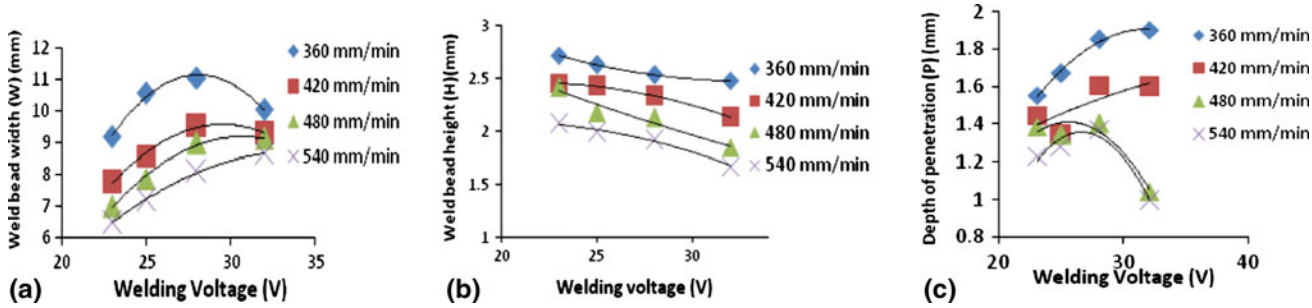

Fig. 5 Effect of welding voltage at different traverse welding speeds on (a) weld bead width, (b) bead height, and (c) depth of penetration

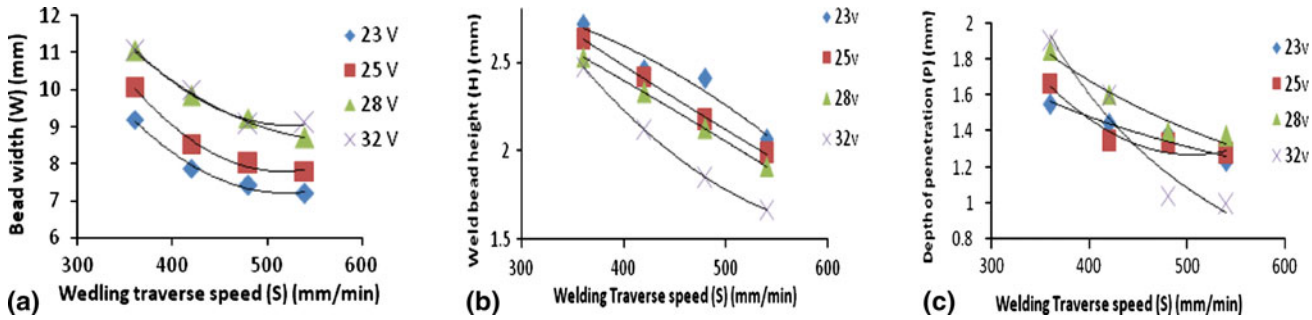

Fig. 6 Effect of traverse welding speeds at different welding voltage on (a) weld bead width, (b) bead height, and (c) depth of penetration

traverse speed, as shown in Fig. 5(b). The effect of the increase in the welding voltage on the depth of penetration is shown in Fig. 5(c). There is no clear correlation between the welding voltage and depth of penetration. The results suggest is that with higher speeds and higher voltages the penetration can be reduced in some circumstances.

The effects of increasing welding traverse speed on the weld bead width are shown in Fig. 6(a). In general, the weld bead width decreases with an increase in the welding traverse speed at all welding voltages. The effects of increasing welding traverse speed on the weld bead height are shown in Fig. 6(b). As can be seen in Fig. 6(b), the increase in the welding traverse speed led to a decrease in the weld bead height. The effects of increasing welding traverse speed on the depth of penetration are shown in Fig. 6(c). There is no clear correlation between the welding traverse speed and the depth of penetration.

Heat input per kilogram of consumable deposited increases with welding voltage and decreases with welding speed. The effects of higher heat input are critical to weld bead geometry. From Fig. 5 and 6, it can be seen that there is a correlation

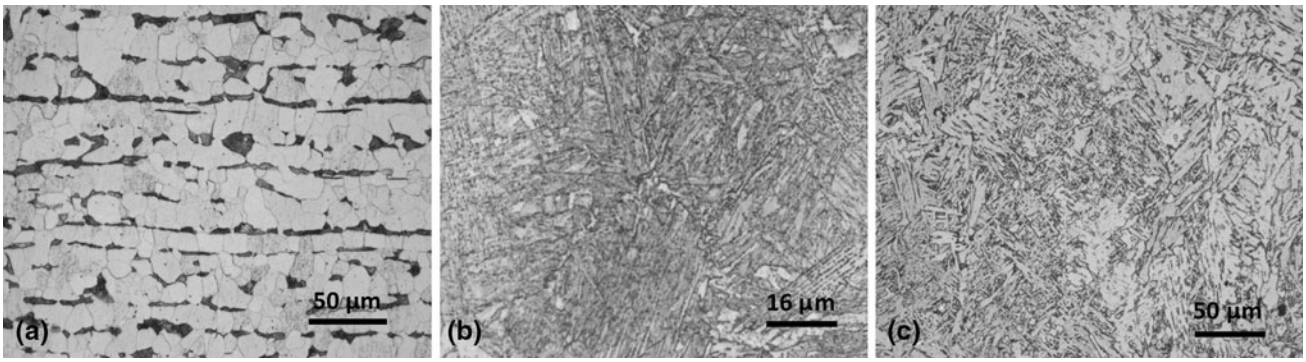

Fig. 7 Microstructures of (a) parent material (b) weld metal, and (c) HAZ

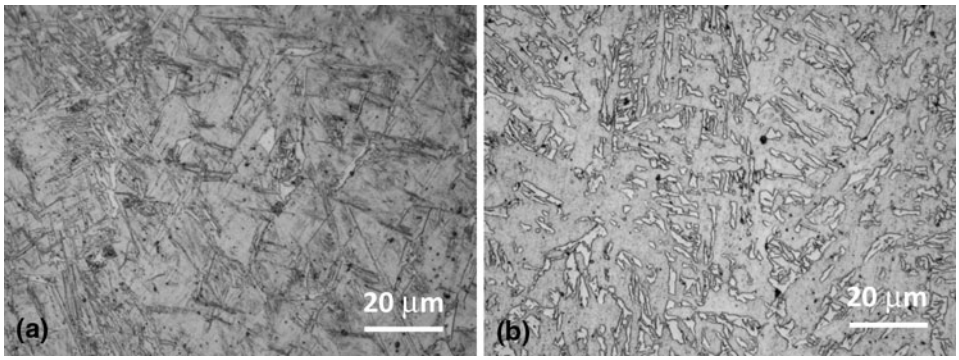

Fig. 8 (a) Microstructure of the HAZ without overlap, bainitic structure (acicular type); and (b) microstructure of the HAZ (same location) after the overlap, partially spherodite bainite ×1000 magnifications

between the heat input and both the weld bead width and height. The increase in the welding heat input leads to an increase in the melted volume under the weld arc and thereby results in an increase in the width and a decrease in the height of the weld pool. However, the depth of penetration does not show a clear trend and penetration at high voltages and weld speed is reduced.

3.2 The Effects of Bead Overlap Percentage

Different percentages of bead overlaps were studied to examine their effects on the mechanical properties as well as the microstructure of the HAZ. In industry, welding repairs tend to be performed using 50% bead overlap, and it is usually achieved by placing the tip of the electrode on the toe of the previous bead (Ref 4). However, there is little research on the justification and validation for the use of this percentage of bead overlap. In this study, the parallel deposition method was used to produce quantitative results with 40-80% overlap as shown in Fig. 2(b). The parallel deposition method used was also to be compared with the results of previous study where the two beads were inclined at an angle to each other and thus varying in percentage overlap (Ref 4). All the samples in this experimental study consisted of two weld beads only. Sections of each percentage of bead overlap were examined to assess the degree of microstructure tempering in the HAZ and to carry out hardness survey.

3.2.1 Microstructure. Various structures across the weldment, namely, the weld metal, parent metal, and HAZ were examined at different magnifications. The microstructure of the parent material, shown in Fig. 7(a) consisted of elongated (in the rolling direction) grains of ferrite and pearlite. The microstructural features in the weld metal and the HAZ regions of the single bead weld (before any deposition sequence) were more clearly revealed at a higher magnification, and were seen to consist of martensite and bainite needles, regardless of the overlap percentages used. The microstructure of the weld metal and HAZ are shown in Fig. 7(b) and (c), respectively. The heat of the subsequent beads and the percentage of overlap were the key factors of microstructure transformation. The increase of overlap percentage increases the degree of refinement. For instance, in the 40% bead overlap, only 40% of the volume of the first bead was covered by the second bead. Consequently, about 40% of the coarse grain in the HAZ was refined and tempered. However, in the sample that was overlapped by 80%, 80% of the microstructure of the first bead was tempered and refined. An illustrative example for the refinement of the HAZ is shown in Fig. 8. The HAZ microstructure was transformed from acicular to spherodite bainite, resulting in hardness reduction as shown in Fig. 9. The tempering, refinements, and the microstructure transformation observations in this were consistent with the previous study (Ref 4). The resultant microstructure was transformed to partially spherodite bainite which has better mechanical properties. This indicates the importance of bead overlap in enhancing the HAZ microstructure.

3.2.2 Hardness. Hardness measurements for different overlap percentages are plotted against their locations. Figure 9 shows the hardness measurements for samples having different percentages of bead overlap ranging from 40% to 80%. It can be seen in this graph that as the percentage of bead overlap increased the hardness in the HAZ is improved on the traverse line which is on Fig. 9. It is also clear from this graph that 80% bead overlap gave the lowest hardness values.

By studying the hardness profiles produced by different percentages of bead overlap, it was observed that the hardness is correlated with the degree of microstructural tempering occurring as a result of bead overlap. The tempered microstructure showed less hardness than the untempered microstructure. For example, bead toes showed high hardness readings when they are not tempered, but these values were decreased significantly when tempering took place.

Both the microstructural and hardness results of this study indicate that the parallel method used in this study is consistent with the inclined method used in the earlier study (Ref 4). On the other hand, increasing bead overlap percentage requires higher amount of weld metal and increasing the overall welding time which leads to the impracticality of high bead overlap percentage (e.g., 70-90%). Therefore, the widely used bead overlap percentage, namely 50%, can be considered to be practically the best option for carrying out welding work.

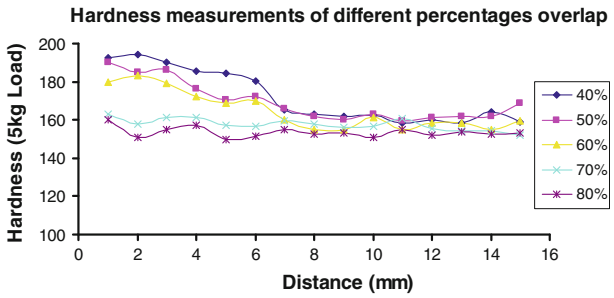

Fig. 9 Hardness profiles for 40-80% bead overlap moving from the center of the first bead to the toe at a distance of 1 mm below the fusion line as shown in Fig. 4(a)

3.3 The Effects of the Deposition Sequence

3.3.1 Microstructure. Full explanation of the microstructure of the deposition sequence can be found elsewhere (Ref 5). In general, the microstructure of the first bead was considerably transformed after the deposition of the second and the subsequent beads. However, the variations in microstructure were also subjected to the sequence of the subsequent beads. The sizes of the refined HAZs obtained using different welding sequences as explained before, were measured using a traveling microscope.

3.3.2 Hardness. Hardness profiles under different welding conditions were generated and plotted in Fig. 10 and 11 for the first and the second deposition sequences, respectively. In both Fig. 10 and 11, (a) represents the hardness profile of a single bead, (b) represents the hardness profiles of two beads, (c) represents the hardness profiles of three beads, and (d) represents the hardness profiles of four beads.

On studying the hardness graphs produced using different welding sequences, it was noticed that the hardness was increased in the areas that are not tempered by a subsequent bead or layer as can be seen in Fig. 10(a) and 11(a). In the case of the samples, which contain a single bead, high hardness values were recorded in the weld beads and the coarse-grained HAZ. However, these values were decreased significantly after depositing the subsequent beads. The deposition directions in both sequences have a direct effect on the percentage of tempering reached. Full explanations can be found in Ref 5.

On studying the HAZ, it was found that the coarse-grained HAZ associated with the first bead of the first sequence was partially refined after depositing the second and the third beads because it is a unidirectional welding (welding going in one direction away from the first bead). On the other hand, the coarse-grained HAZ of the first bead in the second sequence

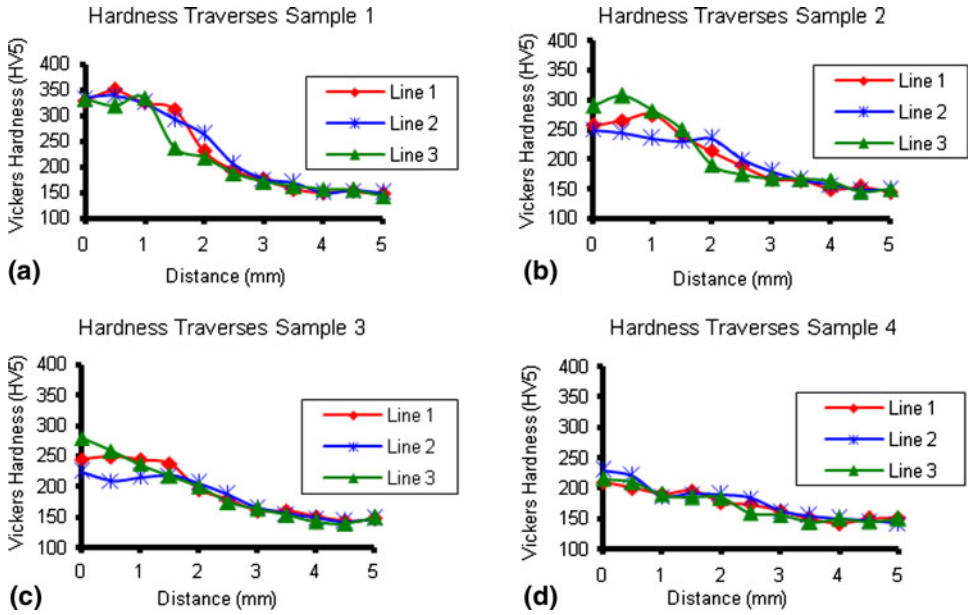

Fig. 10 Hardness traverses of the first deposition sequence as explained in Fig. 4(b)

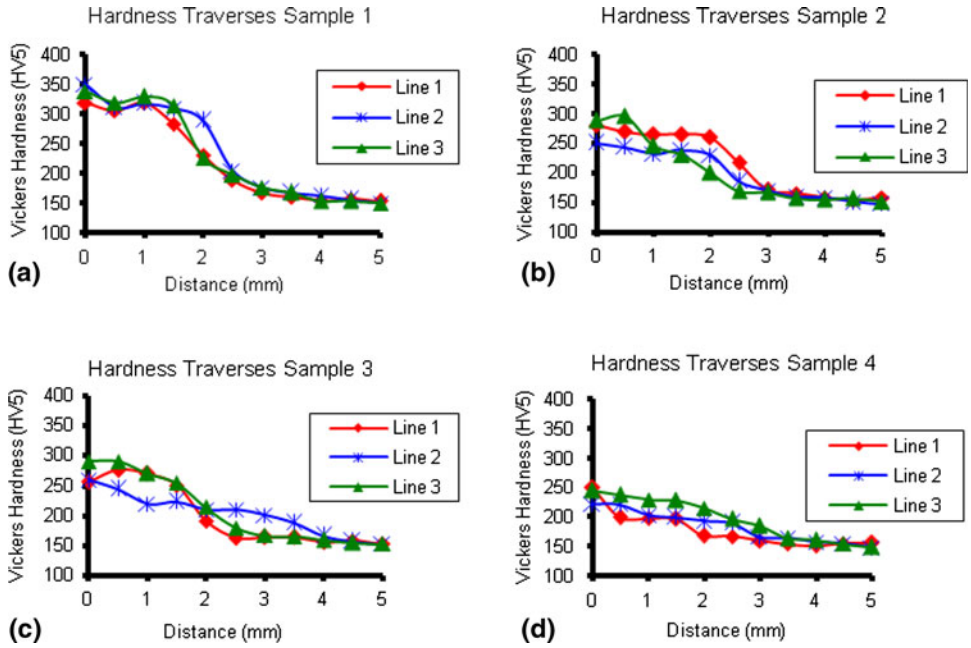

Fig. 11 Hardness traverses of the second deposition sequence as explained in Fig. 4(b)

was fully refined after depositing the left and right beads because it is a bidirectional welding (welding going in two directions, right and left to the first bead).

To show the effectiveness of the deposition sequence, a comparison was made based on the hardness measurements between the first and the second sequence as can be seen in Fig. 10 and 11, respectively. There were no significant differences in the hardness after depositing the subsequent beads and layers in both sequences.

It is clear from the graphs in Fig. 10(b, c) and 11(b, c) that the hardness measurements decreased in both sequences after depositing the subsequent beads. However, there was no significant difference in the hardness of the HAZ obtained using the different welding sequences as can be seen in Fig. 10(d) and 11(d).

4. Conclusion and Recommendation

In this article, an experimental study was conducted to investigate the influence of welding parameters in FCAW process particularly welding voltage and travel speed on weld bead dimensions. In conclusion, it was found that the increase in the welding voltage leads to an increase in the weld bead width, and the increase in the welding traverse speed leads to a decrease in the weld bead width.

The article also examined different percentages of bead overlap and studied their effects on the hardness and the microstructures of the HAZ. Both the microstructural and hardness results of the bead overlap percentages indicate that the parallel method used in this study is consistent with the inclined bead method used in the earlier study (Ref 4). It also indicates that the enhancement of microstructure is achieved with higher percentages of bead overlap. It was also found that the widely used bead overlap percentage, namely 50%, can be considered the most practical option for carrying out welding work.

Two deposition sequences were investigated in this study. This showed that there were no significant differences in the microstructure, hardness, and the size of the refined HAZ between the two deposition sequences. However, a significant improvement in the microstructure and the size of the refined HAZ, and a reduction in the hardness were achieved after depositing the second bead, irrespective of the deposition sequence. The results of the microstructure and hardness for the deposition sequence experiment were consistent with the earlier study (Ref 5). The results of the deposition sequence also suggest that the 100% bead overlap for the second layer with higher heat inputs can give better microstructural refinement.

References

1. K.C. Mitchell, The Applications of Flux Cored Arc Welding (FCAW) in UK Power Plant, *OMMI*, 2003, **2**(1), p 7
2. K.C. Mitchell, Repair Welding in the Power Industry Using Cored Wires, *Proceedings of the 1998 1st IEE/IMechE International Conference on Power Station Maintenance—Profitability Through Reliability*, Mar 30-Apr 1, 1998 (Edinburgh, UK) IEE, Stevenage, England, 1998
3. A. Aloraier, A. Al-Mazrouee, J.W.H. Price, and T. Shehata, Weld Repair Practices Without Post Weld Heat Treatment for Ferritic Alloys and Their Consequences on Residual Stresses: A Review, *Int. J. Pres. Ves. Pip.*, 2010, **87**(4), p 127–133
4. A. Aloraier, R. Ibrahim, and P. Thomson, FCAW Process to Avoid the Use of Post Weld Heat Treatment, *Int. J. Pres. Ves. Pip.*, 2006, **83**(5), p 394–398
5. A.S. Aloraier, R.N. Ibrahim, and J. Ghojel, Eliminating Post-Weld Heat Treatment in Repair Welding by Temper Bead Technique: Role Bead Sequence in Metallurgical Changes, *J. Mater. Process. Technol.*, 2004, **153–154**, p 392–400
6. K. Ishizaki, Interfacial Tension Theory of the Phenomenon of Arc Welding-Mechanism of Penetration, *Proceeding of Symposium on*

Physics of Arc Welding, The Institute of Welding, London, 1962, p 195–209

7. K. Ishizaki, On the Formation of the Weld Bead, *Proceeding of Symposium on Physics of Arc Welding*, The Institute of Welding, London, 1962, p 155–157
8. A. Shumovsky, *Controlling Welding Shrinkage and Distortion*, The Canadian Welder, 1952, p 179–180
9. M.A. Aesh, Optimization of Weld Bead Dimensions in GTAW of Aluminum-Magnesium Alloy, *Mater. Manuf. Process.*, 2001, **16**(5), p 725–736
10. V. Dey, D.K. Pratihar, G.L. Datta, M.N. Jha, T.K. Saha, and A.V. Bapat, Optimization of Bead Geometry in Electron Beam Welding Using a Genetic Algorithm, *J. Mater. Process. Technol.*, 2009, **209**(3), p 1151–1157
11. P. Sathiya, S. Aravindan, A.N. Haq, and K. Paneerselvam, Optimization of Friction Welding Parameters Using Evolutionary Computational Techniques, *J. Mater. Process. Technol.*, 2009, **209**(5), p 2576–2584
12. V.K. Goyal, P.K. Ghosh, and J.S. Saini, Analytical Studies on Thermal Behaviour and Geometry of Weld Pool in Pulsed Current Gas Metal Arc Welding, *J. Mater. Process. Technol.*, 2009, **209**(3), p 1318–1336
13. K.Y. Benyounis and A.G. Olabi, Optimization of Different Welding Processes Using Statistical and Numerical Approaches—A Reference Guide, *Adv. Eng. Softw.*, 2008, **39**(6), p 483–496
14. V. Gunaraj and N. Murugan, Prediction and Comparison of the Area of the Heat-Affected Zone for the Bead-on-Plate and Bead-on-Joint in Submerged Arc Welding of Pipes, *J. Mater. Process. Technol.*, 1999, **95**(1–3), p 246–261